

Article

# An Advanced Sodium-Cooled Fast Reactor Core Concept Using Uranium-Free Metallic Fuels for Maximizing TRU Burning Rate

Wuseong You and Ser Gi Hong \*

Department of Nuclear Engineering, Kyung Hee University, Deogyong-daero, GiHeung-gu, Yongin, Gyeonggi-do 446-701, Korea; wsyou87@naver.com

\* Correspondence: sergihong@khu.ac.kr; Tel.: +82-31-201-2782

Received: 24 October 2017; Accepted: 28 November 2017; Published: 1 December 2017

**Abstract:** In this paper, we designed and analyzed advanced sodium-cooled fast reactor cores using uranium-free metallic fuels for maximizing burning rate of transuranics (TRU) nuclides from PWR spent fuels. It is well known that the removal of fertile nuclides such as  $^{238}\text{U}$  from fuels in liquid metal cooled fast reactor leads to the degradation of important safety parameters such as the Doppler coefficient, coolant void worth, and delayed neutron fraction. To resolve the degradation of the Doppler coefficient, we considered adding resonant nuclides to the uranium-free metallic fuels. The analysis results showed that the cores using uranium-free fuels loaded with tungsten instead of uranium have a significantly lower burnup reactivity swing and more negative Doppler coefficients than the core using uranium-free fuels without resonant nuclides. In addition, we considered the use of axially central  $\text{B}_4\text{C}$  absorber region and moderator rods to further improve safety parameters such as sodium void worth, burnup reactivity swing, and the Doppler coefficient. The results of the analysis showed that the final design core can consume  $\sim 353$  kg per cycle and satisfies self-controllability under unprotected accidents. The fuel cycle analysis showed that the PWR–SFR coupling fuel cycle option drastically reduces the amount of waste going to repository and the SFR burner can consume the amount of TRUs discharged from 3.72 PWRs generating the same electricity.

**Keywords:** sodium-cooled fast reactor (SFR); TRU burning; uranium-free fuel; PWR spent fuel; nuclear fuel cycle

---

## 1. Introduction

Currently, 20 PWRs (Pressurized Water Reactor) and four CANDU (CANadian Deuterium Uranium) reactors are operating in South Korea and their electric capacities are about 22.519 GWe. As of 2016, the electricity generated by nuclear power plants delivers about 30% of the total electricity in South Korea. On the other hand, these nuclear power plants have generated lots of nuclear spent fuels but our country does not have any repository for nuclear spent fuel even if a repository was constructed for low and medium-level waste in Gyeongju. In South Korea, the nuclear spent fuels from PWRs are currently stored in the spent fuel pool storage but it is expected that the capacities of the spent fuel pool storage will be exceeded in the near future. The typical PWR spent fuel of 50 MWD/kg burnup and 10 years cooling is composed of 93.6% uranium isotopes, 1.21% TRU nuclides, and 5.15% fission products. The TRU (Transuranics) nuclides, in spite of their small contents in spent fuel, are considered the most problematic nuclides due to their high radiotoxicities and heat generation over a long time period.

Over the last decades, extensive studies have been performed on partitioning and transmutation (P & T) strategies, which refer to selective separations of nuclides from spent fuel and selective burning or transmutation of them in fission reactors to reduce the radiological burden and heat load of the

spent fuel on geological storage [1–3]. Basically, P & T strategies require the deployment of advanced reprocessing techniques and specifically a high reduction efficiency of radiotoxicity with a factor of 100 requires very small loss fractions of 0.1% during reprocessing and fuel fabrication of recycled fuel. The other requirements of the efficient P & T strategies are an advanced reactor in which fission reactions burn the target nuclides such as TRU and minor actinides (MA) rather than capture reactions to reduce the production of higher mass number actinides and the multi-recycling to almost completely fission the actinides. Previous studies have shown that P & T clearly reduces the actinide inventory in high-level waste (HLW) leading to reductions in the risks arising from less probable increase of actinide mobility in certain geological situations and radiological impact by human intrusion even if radionuclide release from the waste to the environment and related doses to the population are not significantly reduced from P & T.

The burning or incineration of these TRU nuclides using fission reactions in PWRs or fast reactors has been intensively studied for several decades. In particular, liquid metal cooled fast spectrum reactors such as the sodium-cooled fast reactor (SFR) and lead-cooled fast reactor (LFR), coupled with a closed fuel cycle using recycling of actinides, can provide effective burning due to excellent neutronic properties such as a large number of excess neutrons produced by fission and a high fission-to-capture ratio [4–6]. With a closed fuel cycle, the nuclear park, which consists of PWRs and liquid metal cooled fast reactors, significantly reduces the required capacity of the final repositories for the nuclear wastes because only a small fraction of TRU nuclides lost during reprocessing and fuel fabrication go to the repositories and the surplus amount of uranium that is produced from the reprocessing of PWR spent fuel can be utilized in the fast reactors. Specifically, it has been shown that the reduction of radiotoxicities down to the natural radiotoxicity level (i.e., the equilibrium radiotoxicity level of the natural uranium required for LWR fuel fabrication) takes a few hundred-thousands of years, but the separation of TRU and uranium from PWR spent fuel reduces the radiotoxicity of the remaining HLW to the natural radiotoxicity level within a time frame of several hundred years [1,2].

Of the fast spectrum reactors, SFR [7,8] has been considered a more realistic fission system that can burn the TRU feeds from the PWR spent fuel stocks with recycling of actinides than LFRs [9] due to their technical maturity because the other type fast reactors such as lead- and gas-cooled fast reactors have not been constructed and operated as commercial reactors. In particular, it is shown from the operational experience records for the PHENIX, BN-600, and FBTR that SFRs are sufficiently reliable to be operated up to a comparable availability level of LWRs [10]. In addition, SFRs have more than 300 reactor years of practical operation and there have been active research projects for the design and construction of advanced SFRs such as ASTRID in France [11] and PGSFR [12] in South Korea. The sodium-cooled fast reactors for burning TRUs from PWR spent fuels are designed to have a low conversion ratio by reducing fuel volume fraction or reducing neutron leakage or increasing neutron absorption such that a large amount of external TRUs from PWR spent fuel stocks are steadily fed into them and consumed by neutron reactions. However, the typical SFR burners [13–16] have a limited TRU burning rate due to the fact that they use metallic or oxide fuels containing fertile nuclides such as  $^{238}\text{U}$  and  $^{232}\text{Th}$ ; these fertile nuclides generate actinides having higher mass numbers through neutron capture even if they are designed to have a low conversion ratio (e.g., 0.5). To further enhance the TRU burning rate, the removal of the fertile nuclides from the initial fuels is required and it accelerates the reduction of TRUs that are accumulated in LWR spent fuel stocks. However, it is well known that the removal of fertile nuclides from the fuel degrades the inherent safety of the SFR burner cores through the significant decrease of the fuel Doppler effects, the increase of sodium void reactivity worth, the significantly large burnup reactivity swing, and the reduction of the delayed neutron fraction [16–20]. So, the maximization of TRU burning rate requires the development of the advanced core concept, which can minimize the degradations of the inherent safety features without a loss of high TRU burning capability.

In this work, advanced 400 MWe SFR burner cores using metallic uranium-free fuels are designed to maximize the TRU burning rate [20]. These uranium-free fuels are considered by adding resonance

isotopes such as nickel or tungsten instead of fertile materials in metallic fuels of TRU-10Zr to improve the performances of the uranium-free cores. Actually, it is expected that the addition of these resonant nuclides into fuel will reduce the burnup reactivity swing by increasing the heavy metal inventory and improve the Doppler coefficient by increasing the resonance absorption. However, the sodium void reactivity, which is one of the key safety parameters in SFR, is not reduced by adding these resonance nuclides into fuel but increased due to the increase of TRU contents in fuel. So, we introduced an axially central absorber region and moderator rods for each fuel assembly to reduce sodium void reactivity (SVR) and additionally to increase heavy metal (TRU) loading. We expected that the axially central absorber region would reduce the sodium void reactivity worth by increasing the neutron absorption leaking into this absorber region when the sodium coolant is voided and that this absorber region would increase the initial heavy metal inventory for maintaining criticality, which reduces the burnup reactivity swing without a loss of TRU burning rate. The moderator rods are introduced to improve the Doppler effect and to reduce sodium void reactivity by softening the core neutron spectrum. In addition, detailed decomposition analysis of coolant void reactivity based on neutron balance with normalization to the production rate was performed to better understand the effect of coolant voiding on reactivity [13,14,21] and the quasi-static reactivity balance analyses were performed to evaluate the inherent safety features of the cores [4,16,22,23]. Finally, we analyzed the performances for the fuel cycle that is comprised of SFR burners and PWRs to show the mass flows for the actinides and the characteristics of the wastes going to the repository [24]. Section 2 describes the computation methods used in this study, Section 3 gives the design and analysis of advanced SFR reactor cores, and the fuel cycle analysis is given in Section 4. Finally, a summary and conclusion are given in Section 5.

## 2. Computational Methods

A MATXS format 150 group cross section library that was generated by KAERI (Korea Atomic Energy Research Institute) based on ENDF/B-VII.r0 was used as a starting multi-group cross section library for master nuclides, which includes actinides and structural and coolant nuclides. On the other hand, the multi-group cross sections for the fission products were generated using a MATXS format 80 group cross section library prepared based on ENDF/B-VI. Lumped fission product cross sections for each fissionable actinide for taking into account the effect of fission products are generated using the TRANSX code [25] by weighting the microscopic cross sections of the fission products with their fission yields. The TRANSX code is used to generate the ISOTXS format multi-group cross section from the MATXS format library where the Bell–Hansen–Sandmeier method and the Bondarenko method are used for the transport correction and resonance self-shielding treatment, respectively. Then, the core region-wise neutron spectra are obtained by solving the neutron transport equation with DIF3D [26] R-Z model and with a 150 group cross section. Then, these core region-wise neutron spectra are used for TRANSX code to produce the condensed core region wise cross sections. The core depletion analysis was done with the REBUS-3 [27] equilibrium model, while the neutron diffusion equation is solved with the HEX-Z nodal option and 9 group cross section library. The core physics parameters were evaluated with 80 group cross sections and DIF3D HEX-Z nodal option. The decay chain spans the range from  $^{232}\text{Th}$  to  $^{246}\text{Cm}$ . In the REBUS-3 equilibrium model, the TRU contents in the charging fuel are automatically searched such that  $k_{\text{eff}}$  at EOEC (End of Equilibrium Cycle) is 1.005. At EOEC, the 1/(number of batches) of the fuel inventory are discharged from the core and sent to the reprocessing plant after cooling for 365 days. We assumed 99.9% and 5% recoveries for actinides and rare earth fission products, respectively, during reprocessing and the other fission products are assumed to be completely removed to the waste stream during reprocessing. The reprocessed fuels are sent to the fuel fabrication plant, where the reprocessed fuel materials are mixed with TRUs recovered from PWR spent fuel stocks. In this work, we assumed eight months' reprocessing and eight months' fuel fabrication, which are followed by two months' pre-storage before loading into the core. The composition of TRU feed used in this work is the TRU composition of LWR spent fuel having 50 MWD/kg and 10 years' cooling.

### 3. Core Design Study and Performance Analysis

#### 3.1. Reference Core Design

The reference core is selected from our previous studies [20]. The reference core rate is 400 MWe, which corresponds to 1015.6 MW thermal output with 39.4% efficiency. The configuration is shown in Figure 1. The core consists of two different type fuel assemblies that were devised to achieve power flattening with a single feed fuel composition in our previous studies. The normal fuel assemblies, comprised of 271 fuel pins within a normal hexagonal duct of 3.7 mm thickness, are loaded in the outer region, while the fuel assemblies having 217 fuel pins within 11.5 mm thick ducts are in the inner core.

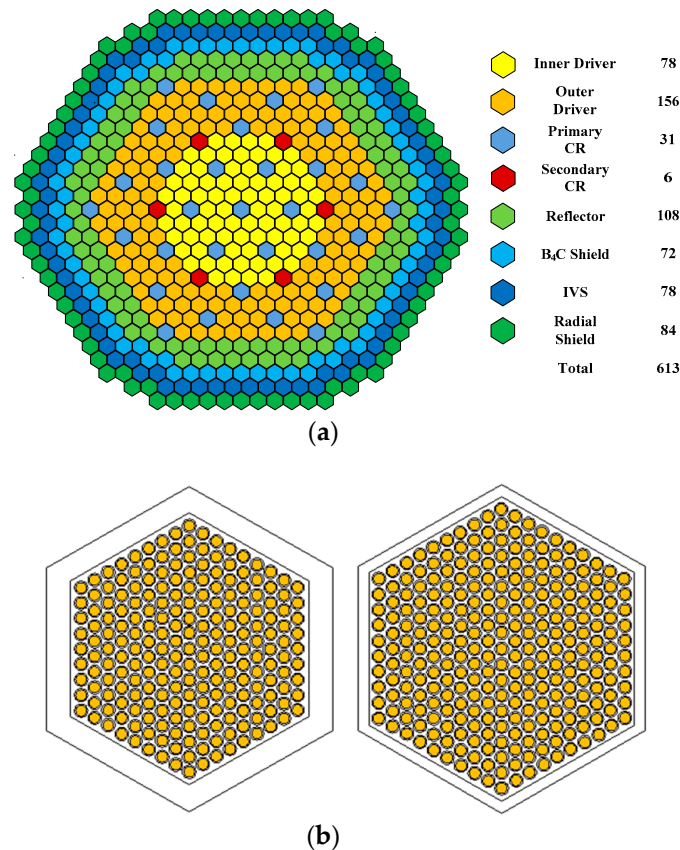


**Figure 1.** Configuration of the reference core and fuel assemblies. (a) Core configuration; (b) fuel assembly configurations (left: thick duct assembly, right: normal duct assembly).

Table 1 summarizes the main design parameters of the cores. The active core is 90 cm high at cold state. The outer diameter of fuel rod is 7.5 mm and clad thickness is 0.53 mm. The average linear heat generation rate is 190.6 W/cm. For this reference core configuration, three different ternary metallic fuels (i.e., TRU-U-10Zr, TRU-Ni-10Zr, and TRU-W-10Zr) and one binary metallic fuel (i.e., TRU-Zr) are considered to be tested and the performances of the cores loaded with these fuels are analyzed and inter-compared. In particular, the fertile metallic ternary fuel of TRU-U-10Zr was considered to compare the TRU burning capability of the core loaded with fertile metallic fuel with ones loaded with fertile-free fuels while the binary fuel of TRU-Zr to show the degradation of the Doppler effects and burnup reactivity swing for this binary fueled core. A 75% smear density of all the considered fuels is considered to cope with swelling of the metal fuel slugs and the sodium is filled into the gap between the fuel slug and cladding. As the fuel burnup proceeds, the metallic fuel slug expands outwardly, which leads to the lift up of the sodium in the gap into the 170 cm upper gas plenum region. The axial configuration of the reference core is shown in Figure 2. The lifted up sodium is assumed to fill an

18 cm high region (this region is designated by 'Bond' in Figure 2) of the upper gas plenum. On the other hand, the region below the fuel is the lower shield. In this work, all the structural material including cladding is assumed to be HT9.

**Table 1.** Main design parameters of the reference core.

Design Parameter	Specification
Power (MWe/MWt)	400/1015.6
Fuel type	TRU-Ni(or W)-10Zr
Smear density of fuel	75%
Number of rods per FA (outer/inner)	271/217 <sup>a</sup>
Smear density of fuel	75%
Active core height (cm)	90
Duct wall thickness (mm, outer/inner)	3.7/11.5 <sup>a</sup>
Assembly pitch (cm)	16.22
Rod outer diameter (mm)	7.5
Wire wrap diameter (mm)	1.4
Clad thickness (mm)	0.53
Fuel cycle length (EFPD)	332
Average heat generation rate (W/cm)	177
Number of fuel management batches	4
Volume fraction (fuel/coolant/structure, %)	
Inner core	30.6/30.8/38.6
Outer core	38.3/36.9/24.8

<sup>a</sup> Values for the normal and new assemblies, respectively.

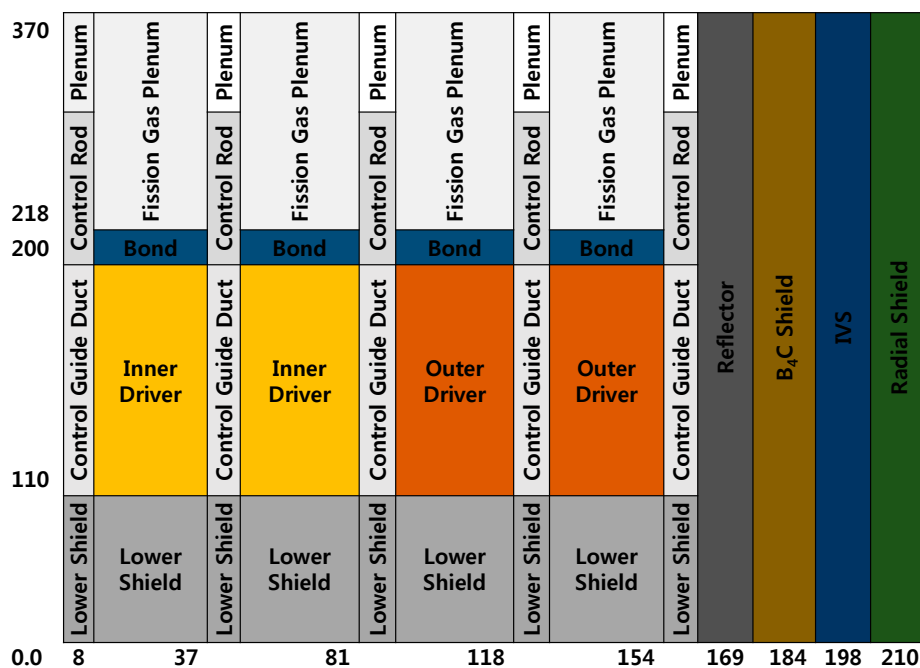


**Figure 2.** Axial configuration of the reference core.

As shown in Figure 1, the active core consists of 234 fuel assemblies that are surrounded by two rings of reflector assemblies composed of 75.43 % Inconel-600, 15.82 % coolant, and 8.75 % HT9. The reflector assemblies are sequentially followed by B<sub>4</sub>C shield, in-vessel storage (IVS), and radial shield assemblies. The reactivity control system consists of two separate control rod groups (i.e., primary and secondary groups comprised of 31 and six control rod assemblies, respectively). A large

number of primary control rod assemblies were considered to cope with the large burnup reactivity swing that may be expected in the burner cores. The primary control rod assemblies should be able to shut down the reactor from any operating condition including overpower condition to the refueling condition with one stuck rod assembly of the largest reactivity worth and also compensate for the reactivity effect of the fuel cycle or fuel burnup. Boron carbide ( $B_4C$ ) was used as the neutron absorber in the control rods. The cycle length is 332 effective full power days (EFPD) and a four-batch fuel management scheme is used for both inner and outer core regions.

Table 2 compares the performances of the cores using four different metallic fuels described above. Table 2 shows that the reference core using TRU-U-10Zr fuel has a high cycle average TRU conversion ratio of 0.85 and so a low TRU transmutation rate of 69 kg/cycle because this reference core has no way to reduce the conversion ratio except for use of the thick duct assemblies in inner core region, while this core has a small burnup reactivity of 1452 pcm due to the high conversion ratio, which reduces the reactivity control requirement by the control rod assemblies. The cycle average TRU conversion ratio is the ratio of the produced amount of TRUs to the destructed one of TRUs over the cycle. In comparison with the reference core loaded with fertile metallic fuel (i.e., TRU-U-10Zr), the cores using uranium-free fuels have much larger TRU consumption rates of ~350 kg/cycle because they use fertile-free fuels. These TRU consumption rates correspond to a TRU support ratio of ~4.2, which means that these cores loaded with uranium-free fuels (i.e., TRU-Zr, TRU-Ni-10Zr, and TRU-W-10Zr) can consume the amount of TRUs discharged from ~4.2 PWRs of the same thermal power and cycle length. However, these cores have much larger burnup reactivity swings than the reference core due to their poor breeding of fissile materials (note that they have much smaller TRU conversion ratio of ~0.43) and to their low heavy metal inventories. Of these cores using uranium-free fuels, the core using binary metallic fuel (i.e., TRU-Zr) has the largest burnup reactivity swing of 7193 pcm due to the highest average discharge burnup (i.e., lowest initial heavy metal inventory), while the cores using nickel-based fuel (i.e., TRU-Ni-10Zr) and tungsten-based fuel (i.e., TRU-W-10Zr) have a smaller burnup reactivity swing of 6740 pcm and 5606 pcm, respectively, due to their larger heavy metal inventories because nickel and tungsten isotopes have a higher absorption cross section than zirconium isotopes. So, the core using TRU-Zr fuel requires a large amount of control rod assembly reactivity, which makes it difficult to operate the reactor.

**Table 2.** Summary of the reference core performances having different metallic fuels.

Parameter	TRU-U-10Zr	TRU-Zr	TRU-Ni-10Zr	TRU-W-10Zr
Burnup reactivity swing (pcm)	1452	7193	6740	5606
Average discharge burnup (MWD/kg)	114	256	240	193
TRU support ratio	0.837	4.23	4.26	4.29
Cycle average TRU conversion ratio	0.85	0.43	0.44	0.43
TRU consumption rate (kg/cycle)	69.0	349.0	351.0	354.0
Fuel inventories (kg, BOEC/EOEC)				
TRU	3783/3715	4469/4123	4833/4485	6162/5812
U, Ni, or W	14,246/13,969	N/A	7124/7124	11,801/11,801
Zr	2063/2063	5389/5389	1402/1402	2075/2075
Total fuel	20,092/19,747	9858/9512	13,432/13,083	20,169/19,817
TRU contents in Fuel (wt %,BOEC/EOEC)	18.8/18.8	45.3/43.3	36.0/34.3	30.6/29.3
Average linear power (W/cm)	190.6	190.6	190.6	190.6
3D power peaking factor	1.60/1.58	1.52/1.47	1.56/1.51	1.54/1.49
Peak linear power density (W/cm)	304/301	289/280	371/359	366/355
Fast neutron fluence (n/cm <sup>2</sup> )	$3.02 \times 10^{23}$	$3.27 \times 10^{23}$	$2.97 \times 10^{23}$	$2.60 \times 10^{23}$

Therefore, from the point of view of burnup reactivity swing, TRU-W-10Zr fuel is a good candidate for the SFR burner having high TRU burning rate. Figure 3 compares the capture cross sections of a major Ni isotope (i.e.,  $^{58}Ni$ ), a major tungsten isotope (i.e.,  $^{128}W$ ),  $^{90}Zr$ , and  $^{238}U$ . As shown in Figure 3, the resonance isotopes that are considered to be added into fuel have a much higher capture cross section than  $^{90}Zr$  even if  $^{90}Zr$  also has resonance capture. In particular, it is noted that  $^{128}W$  has high resonance cross sections and overall high capture cross sections compared to those of  $^{238}U$ , which

is why we considered tungsten as the resonance material. The neutron spectra of the cores using different fuels are compared in Figure 4, which shows that the core using tungsten-based metallic fuel has the hardest spectrum and the core using nickel-based metallic fuel has a more or less soft spectrum because the nickel isotopes have high energy resonances.

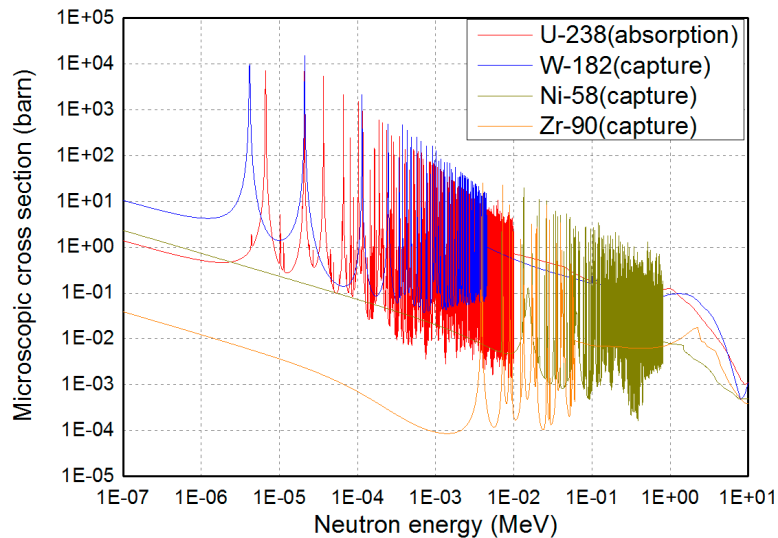


**Figure 3.** Comparison of the microscopic capture (absorption) cross sections for several resonance isotopes.

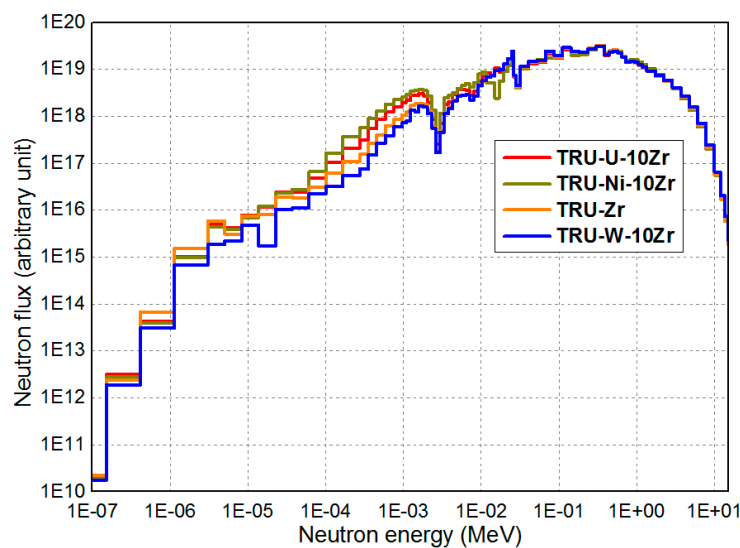


**Figure 4.** Comparison of the neutron spectra for the different metallic fueled cores.

Table 3 compares the reactivity coefficients at the beginning of equilibrium cycle (BOEC) for the reference core using the different metallic fuels. The fuel Doppler coefficients are decomposed into the TRU and non-TRU nuclides (i.e., U, Ni, W, Zr) to better understand the contributions of these nuclides. For the TRU-U-10Zr fueled case, this decomposition shows that TRU nuclides gives a slightly positive contribution ( $\sim 0.0063$  pcm/K), while the main negative reactivity is contributed by  $^{238}\text{U}$ . On the other hand, the TRU-Zr fueled case has only a very small negative Doppler coefficient of  $-0.0628$  pcm/K due to the removal of  $^{238}\text{U}$  and the addition of Ni gives a slightly more negative Doppler coefficient of  $-0.0887$  pcm/K than the TRU-Zr fueled one, while the TRU-W-10Zr fueled case in spite of its large

fuel inventory has a much more negative Doppler coefficient than the TRU-Zr fueled core due to the high resonance capture cross sections of tungsten nuclides.

**Table 3.** Comparison of the reactivity coefficients of the reference cores using different metallic fuels (BOEC).

Parameter	TRU-U-10Zr	TRU-Zr	TRU-Ni-10Zr	TRU-W-10Zr
Fuel Doppler coefficient (pcm/K, 900 K)				
Total fuel	−0.45209	−0.06281	−0.08877	−0.18938
TRU	0.00633	−0.04868	−0.08421	0.00347
Non TRU(U, Ni, W, or Zr)	−0.45591	−0.00020	−0.00005	−0.18826
Radial expansion coefficient (pcm/K)	−0.813	−0.941	−0.823	−0.761
Fuel axial expansion coefficient (pcm/K)				
Fuel only	−0.377	−0.376	−0.339	−0.368
Sodium void worth (pcm, BOEC)	1810(5.5\$)	1102(4.3\$)	1421(5.4\$)	2276(9.6\$)
Control rod worth (pcm, BOEC)				
Primary	15,237(46\$)	19,208(75\$)	16,578(63\$)	13,004(54\$)
Secondary	4112(12\$)	5100(20\$)	4411(16\$)	3516(14\$)
Effective delayed neutron fraction (BOEC)	0.00332	0.00255	0.00260	0.00237

In Table 3, it is noted that the TRU-W-10Zr fueled case has considerably less negative reactivity coefficient by radial expansion of the core support plate and higher sodium void worth, which resulted from its higher capture probability (i.e., smaller leakage probability) than the other cases. As expected, the fertile-free fueled cases have significantly smaller effective delayed neutron fractions than the reference TRU-U-10Zr fueled case, which makes it difficult to control the reactivity change transients. Differently from the expectation that the TRU-Zr fueled case would have higher sodium void worth, this case has the smallest sodium void worth, which resulted from the smaller capture rates for this case due to the small capture cross sections of zirconium isotopes and from the smallest actinide inventory. This phenomenon was analyzed in the following using the decomposition method of sodium void worth based on the neutron balance analysis [13,14,21]. The reactivity change resulted from sodium coolant voiding can be analyzed using the decomposition method based on the neutron balance. The reactivity change using the neutron balance is given by

$$\delta\rho = -\delta l - \delta c - \delta f + \delta n, \quad (1)$$

where  $l$ ,  $c$ ,  $f$ , and  $n$  represent the normalized leakage, capture, fission, and (n,2n) reaction rates, respectively. The normalization is done to the one neutron produced by fission. The variation of the normalized fission rate can be further decomposed into the fission and fission production components as follows:

$$-\delta f = -\delta\left(\frac{F}{F_p}\right) = -\frac{\delta F}{F_p} + \frac{F}{F_p} \frac{\delta F_p}{F_p}, \quad (2)$$

where  $F$  and  $F_p$  represent the un-normalized fission and fission production rates, respectively. So, the final equation for the reactivity change is given by

$$\delta\rho = -\delta l - \delta c - \frac{\delta F}{F_p} + \frac{F}{F_p} \frac{\delta F_p}{F_p} + \delta n. \quad (3)$$

In Equation (2), the first term represents the negative contribution to the reactivity by fission via absorption while the second term represents the positive contribution by fission via production. The results of the sodium void worth decomposition analysis at BOEC are summarized in Table 4.

**Table 4.** Normalized reaction rates and decomposition of sodium void reactivity worth of the reference cores using different metallic fuels (BOEC).

Components	TRU-Zr			TRU-Ni-10Zr			TRU-W-10Zr		
	Reference	Voided	Reactivity (pcm)	Reference	Voided	Reactivity (pcm)	Reference	Voided	Reactivity (pcm)
Leakage	0.2933	0.3214	−2806.3	0.2449	0.2667	−2184.2	0.2131	0.2284	−1529.8
Radial	0.1286	0.1354	−682.1	0.1106	0.1160	−539.1	0.0959	0.0988	−293.2
Axial	0.1648	0.1860	−2124.2	0.1342	0.1507	−1645.1	0.1172	0.1296	−1236.6
Fission	0.3332	0.3326	60.0	0.3336	0.3331	49.7	0.3333	0.3330	36.9
Fission A <sup>a</sup>	N/A	N/A	−64	N/A	N/A	−65.9	N/A	N/A	−43.3
Fission B <sup>b</sup>	N/A	N/A	124.7	N/A	N/A	115.8	N/A	N/A	80.3
Capture (n,2n)	0.2985	0.2600	3847.9	0.3532	0.3176	3555.1	0.3981	0.3604	3766.9
Total sum (reactivity)	0.0004	0.0004	−2.8	0.0003	0.0003	−1.4	0.0010	0.0011	−5.5
		1105			1422			2271	

<sup>a</sup> The third term in Equation (3), <sup>b</sup> The fourth term in Equation (3).

As shown in Table 4, the TRU-Zr fueled case has the highest leakage probability of ~29.3% at the normal state (i.e., no sodium voiding) and the leakage probability increases up to ~32.1% by sodium voiding, which leads to the largest negative reactivity contribution of −2806 pcm. For this case, the positive reactivity contribution of 3848 pcm by the reduction of capture probability under sodium voiding is the largest due to the high TRU inventory in the fuel but the large negative contribution from leakage increase offsets the positive contribution from the capture decrease, which leads to the smallest sodium void worth. The largest sodium void worth of the TRU-W-10Zr case results from the smallest negative contribution by leakage increase and large positive contribution by capture decrease. For all the cases, the contributions by fission to the sodium void worth are small and they range from 37~60 pcm. The contribution from fission via absorption (designated by “Fission A” in Table 4) is negative (−43~−64 pcm), while that from fission via production is positive (80~125 pcm).

The mass flows of TRU nuclides for the cases using TRU-U-10Zr and TRU-W-10Zr fuels are compared in Table 5. Table 5 shows that the case using fertile metallic fuel (i.e., TRU-U-10Zr) consumes 6% (55.5 kg) and 16% (12.3 kg) of their initial charged plutonium and minor actinides’ inventories, respectively, while the one using fertile-free fuel (i.e., TRU-W-10Zr) consumes a much higher amount of plutonium and minor actinides of 21% (295.8 kg) and 20% (54.4 kg), respectively. In comparison with the case using TRU-U-10Zr fuel, the one using TRU-W-10Zr significantly consumes all the plutonium isotopes except for a small increase of <sup>242</sup>Pu and all the minor actinides’ masses are reduced except for <sup>242</sup>Cm and <sup>244</sup>Cm.

**Table 5.** Mass flows of TRU nuclides for the reference cores using TRU-U-10Zr and TRU-W-10Zr fuels (kg).

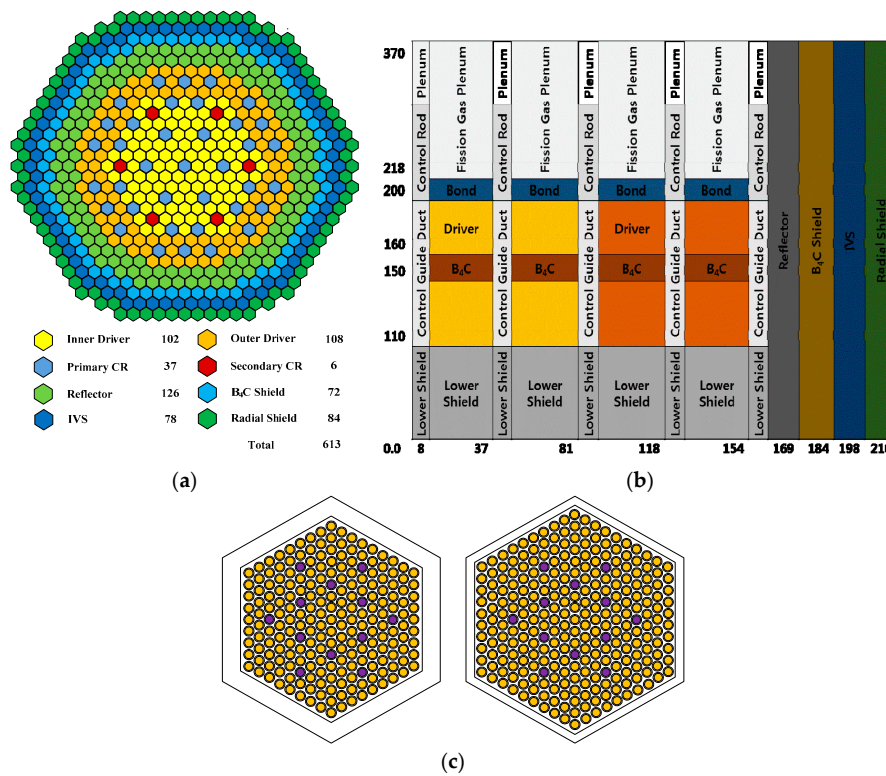
Components	TRU-U-10Zr			TRU-W-10Zr		
	Charge	Discharge	Increase	Charge	Discharge	Increase
Pu-238	29.31	26.64	−2.67 (−9.1%)	112.93	101.18	−11.75 (−10.4%)
Pu-239	486.58	450.73	−35.85 (−7.4%)	477.73	292.71	−185.02 (−38.7%)
Pu-240	310.21	292.58	−17.63 (−5.7%)	651.19	561.56	−89.63 (−13.8%)
Pu-241	37.52	38.14	0.63 (1.7%)	90.62	81.10	−9.52 (−10.5%)
Pu-242	31.07	31.10	0.03 (0.1%)	76.79	76.86	0.08 (0.1%)
Total Pu	894.68	839.18	−55.50 (−6.2%)	1409.25	1113.41	−295.83 (−21.0%)

Table 5. Cont.

Components	TRU-U-10Zr			TRU-W-10Zr		
	Charge	Discharge	Increase	Charge	Discharge	Increase
Np-237	16.66	11.76	−4.90 (−29.4%)	74.92	49.89	−25.03 (−33.4%)
Am-241	35.04	27.19	−7.85 (−22.4%)	113.86	86.34	−27.52 (−24.2%)
Am-242m	2.17	2.16	−0.01 (−0.6%)	7.08	7.01	−0.07 (−0.9%)
Am-243	11.56	10.45	−1.11 (−9.6%)	38.63	32.96	−5.67 (−14.7%)
Cm-242	0.03	1.25	1.23 (4702.2%)	0.08	3.65	3.57 (4673.7%)
Cm-243	0.10	0.11	0.003 (2.6%)	0.29	0.29	−0.001 (−0.5%)
Cm-244	7.31	7.66	0.35 (4.8%)	24.28	24.72	0.44 (1.8%)
Cm-245	2.37	2.35	−0.03 (−1.1%)	7.76	7.62	−0.14 (−1.8%)
Cm-246	1.36	1.36	−0.003 (−0.2%)	4.49	4.47	−0.02 (−0.4%)
Total MA	76.60	64.28	−12.32 (−16.1%)	271.39	216.95	−54.44 (−20.1%)
Total TRU	971.29	903.47	−67.82 (−7.0%)	1680.63	1330.36	−350.27 (−20.8%)

### 3.2. Advanced Uranium-Free Fueled Burner Cores

In this section, we designed and analyzed cores having an axially central  $B_4C$  absorber region in order to reduce the sodium void worth and burnup reactivity swing by increasing fuel loading. In spite of high sodium void worth, the TRU-W-10Zr ternary metallic fuel is considered to be loaded in this core because it significantly reduces burnup reactivity swing and gives a negative Doppler coefficient. The height of the axially central absorber region is considered as a design parameter. Figure 5 shows the radial core loading pattern and the axial configuration including the axial absorber region. As in the reference core described in Section 3.1, the core consists of inner and outer regions that are loaded with thick duct assemblies and normal ones. However, 12  $ZrH_{1.8}$  moderator rods are used in all the fuel assemblies to further reduce the sodium void worth and improve the Doppler coefficient by softening the neutron spectrum. On the other hand,  $ZrH_{1.8}$  has low thermal stability issues but the literature shows that these issues can be solved with the use of yttrium hydride, which is thermally stable up to 1300 °C and has similar neutronic effects to zirconium hydride [10,28]. In addition, the active core height is reduced from 90 cm to 80 cm to reduce sodium void worth. The natural boron was considered in the  $B_4C$  absorber. We also considered the depletion of boron-10 by adding a simple depletion chain by considering the  $(n,\alpha)$  reaction of B-10. The average linear heat generation rate is fixed to 259 W/cm and the active core height is fixed to 80 cm when the height of the  $B_4C$  absorber region changes. As in the reference core, all the cores considered in this section use the same four-batch refueling scheme and the same cycle length of 332 EFPDs.



**Figure 5.** Configurations of the cores having axially central B<sub>4</sub>C absorber region and fuel assemblies: (a) Core configuration; (b) axial core configuration; (c) fuel assembly configurations having 12 ZrH<sub>1.8</sub> moderator rods.

Table 6 summarizes the performances of the cores having different heights of the B<sub>4</sub>C absorber region and compares them. For comparison, we also considered a core having no B<sub>4</sub>C absorber region (designated by Case I in Table 6) and this core uses TRU-W-10Zr fuel and new fuel assemblies having 12 ZrH<sub>1.8</sub> moderator rods.

**Table 6.** Performances of the cores having different axial B<sub>4</sub>C absorber region heights.

Items	Case I	Case II	Case III	Case IV	Case V
Height of B <sub>4</sub> C absorber region (cm)	No absorber	10.0	11.4	13.3	16.0
Average linear power (W/cm)	259	259	259	259	259
Burnup reactivity swing (pcm)	5824	4196	4150	4104	4088
Average discharge burnup (MWD/kg)	206	170	167	164	161
TRU support ratio	4.28	4.28	4.28	4.28	4.28
Average TRU conversion ratio	0.446	0.428	0.425	0.423	0.420
TRU consumption rate (kg/cycle)	352.9	352.9	353.0	353.0	353.0
Fuel inventories (kg, BOEC/EOEC)					
TRU	5833/5482	7202/6851	7331/6979	7486/7135	7651/7300
W	7293/7293	5934/5934	5805/5805	5649/5649	5485/5485
TRU/(TRU+W) (wt %,BOEC/EOEC)	44.4/42.9	54.8/53.6	55.8/54.6	57.0/55.8	58.2/57.1
B-10 inventories (kg, BOEC/EOEC)	-	58.1/53.1	68.5/63.1	83.5/77.7	106.0/99.9
Peak LPD(W/cm, BOEC)	378	378	383	394	412
3D power peaking factor	1.46	1.46	1.48	1.52	1.59
Fast neutron fluence (n/cm <sup>2</sup> )	2.58 × 10 <sup>23</sup>	2.18 × 10 <sup>23</sup>	2.18 × 10 <sup>23</sup>	2.19 × 10 <sup>23</sup>	2.21 × 10 <sup>23</sup>
Sodium void worth(pcm)	1437/1582 <sup>a</sup>	1349/1452	1252/1347	1117/1198	939/998
Control assembly worth(pcm)					
Primary control rod insertion	14,758	12,024	11,703	11,299	10,839
Secondary control rod insertion	2607	2150	2096	2027	1947
Effective delayed neutron fraction β <sub>eff</sub>	0.002452	0.002331	0.002326	0.002322	0.002319
Reactivity coefficients (pcm/K)					
Fuel Doppler (900 K)	-0.371/-0.413 <sup>a</sup>	-0.220/-0.240	-0.211/-0.229	-0.201/-0.217	-0.191/-0.204
Radial expansion	-0.683/-0.742	-0.772/-0.814	-0.806/-0.850	-0.852/-0.898	-0.914/-0.963
Axial expansion	-0.389/-0.427	-0.336/-0.361	-0.306/-0.329	-0.292/-0.333	-0.276/-0.295
Coolant expansion	0.4245/0.464	0.378/0.402	0.347/0.367	0.305/0.319	0.253/0.256

<sup>a</sup> BOEC/EOEC.

As shown in Table 6, the use of the  $B_4C$  absorber region not only significantly reduces the burnup reactivity swings but also considerably reduces the sodium void worth. As mentioned before, the reduction of burnup reactivity swing resulted from the increase of the initial heavy metal loading (i.e., TRU loading) to compensate the reactivity loss due to the neutron capture by the  $B_4C$  absorber region. For example, the core having 10 cm high  $B_4C$  absorber region has a smaller burnup reactivity by 1628 pcm (i.e., ~28%) and a smaller sodium void worth by 88 pcm (~6%) than the core having no  $B_4C$  absorber region (i.e., Case I). Especially, the core having 16cm high  $B_4C$  absorber region (Case V) has a further reduced values of burnup reactivity swing and sodium void worth by 1736 pcm and 498 pcm, respectively, in comparison with the core having no  $B_4C$  absorber region. The Case V core has a higher TRU inventory at BOEC by 31.2% but a lower average discharge burnup by 21.8% than the Case I core having no  $B_4C$  absorber region. The fuel Doppler coefficient becomes less negative as the  $B_4C$  absorber region becomes thicker due to the reduction of tungsten content in fuel, while a thicker  $B_4C$  absorber region leads to more negative reactivity coefficients by radial expansion of the core support plate and by the fuel axial expansion due to the increase of the axial neutron leakage and to the smaller reactivity worth of control rod assemblies due to larger neutron absorption in the  $B_4C$  absorber region. Also, it is noted in Table 6 that the reactivity coefficients by the Doppler effect, radial expansion of core support structure, and fuel axial expansion at EOEC are slightly more negative than those at BOEC. In particular, this trend in the Doppler coefficient is different from that of the typical fertile metallic fueled cores for breeding, in which the main cause for the Doppler coefficient change as fuel burnup is the reduction of  $^{238}U$  content in the fertile metallic fueled core. On the other hand, the sodium void worth and the reactivity coefficient by coolant expansion at EOEC are more positive than those of BOEC, which may also result from the reduction of odd mass number Pu isotope contents at EOEC. Figure 6 shows the axial power distribution (i.e., the plane average volumetric power densities) of the core having a 16cm high  $B_4C$  absorber region (Case V). Figure 6 shows that, as expected, the use of an axial absorber region leads to a distortion of the axial power distribution, which leads to a decrease in sodium void worth in comparison with the core having no  $B_4C$  absorber region (Case I) due to the absorption increase of the leaking neutrons from the core by the  $B_4C$  absorber region.

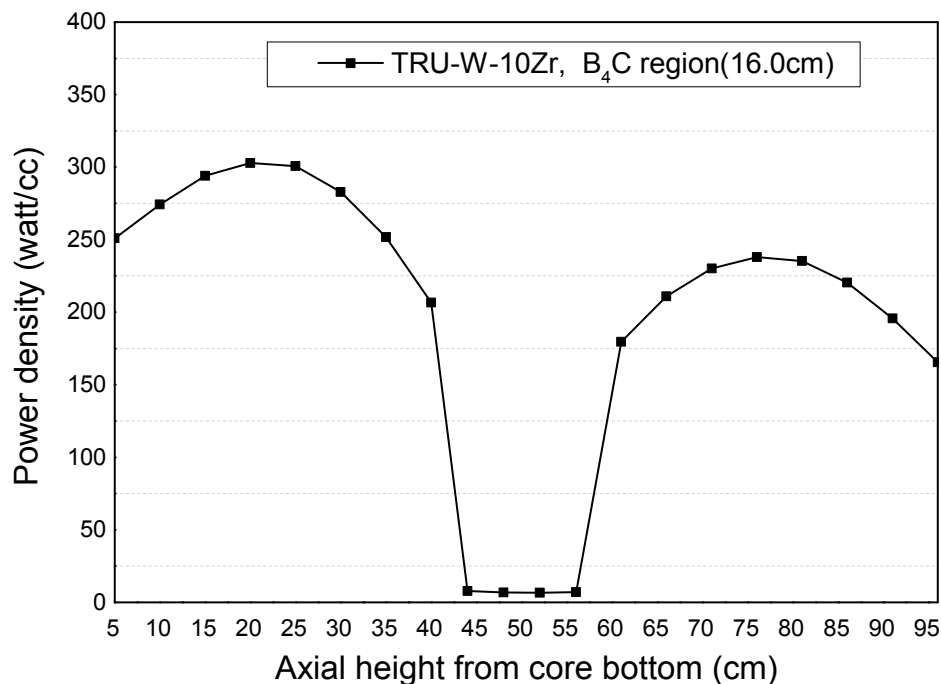


**Figure 6.** Axial power distribution of the core having TRU-W-10Zr with axial central  $B_4C$  absorber regions (BOEC, Height of  $B_4C$  = 16.0 cm)

Next, the decomposition analysis of the sodium void worth for these cores is performed to understand the effects of the axial B<sub>4</sub>C absorber region on the sodium void worth. Table 7 compares the results of the decomposition analysis. From Table 7, it is shown that the use of thicker B<sub>4</sub>C absorber region leads to the smaller negative contributions by the leakage increase but to the smaller positive contributions by the capture decrease, which causes a smaller sodium void worth for the cores having axial B<sub>4</sub>C absorber region. Figure 7 shows the nuclide-wise contributions by fission and capture reactions to the sodium void reactivity worth for the uranium-free fueled cores at BOEC. From this figure, it is shown that the use of axial B<sub>4</sub>C absorber region leads to less positive contributions by fission and capture as mention above. And this figure shows that the absorption increase by <sup>10</sup>B of the B<sub>4</sub>C absorber region under sodium voiding contributes to the sodium void by ~−250 pcm. This less positive contribution for the core using the B<sub>4</sub>C absorber region is larger than for the core using no B<sub>4</sub>C absorber region due to its harder neutron spectra. Figure 8 shows the neutron spectra of the cores. As shown in Figure 8, the tungsten-based fueled core with 16.0 cm B<sub>4</sub>C absorber region has a much harder spectrum than the tungsten-based fueled core with no absorber region due to further capture of the low-energy neutrons by the absorber.

**Table 7.** Normalized reaction rates and decomposition of sodium void worth of the cores having different axial B<sub>4</sub>C absorber region heights.

Components	No Absorber Region		10.0 cm		11.4 cm		13.3 cm		16.0 cm	
	Reference	Reactivity (pcm)	Reference	Reactivity (pcm)	Reference	Reactivity (pcm)	Reference	Reactivity (pcm)	Reference	Reactivity (pcm)
Total Leakage	0.1994	−1147.8	0.1902	−741.7	0.1895	−724.8	0.1885	−709.3	0.1874	−697.2
Radial	0.0928	−158.3	0.0832	−101.9	0.0825	−102.2	0.0816	−104.7	0.0807	−110.8
Axial	0.1066	−989.6	0.1069	−639.8	0.1070	−622.5	0.1069	−604.6	0.1067	−586.4
Fission	0.3326	35.2	0.3317	36.3	0.3316	37.1	0.3315	37.9	0.3314	39.1
Fission A	N/A	−32.9	N/A	−38.3	N/A	−37.0	N/A	−35.1	N/A	−32.2
Fission B	N/A	68.1	N/A	74.7	N/A	74.2	N/A	73.1	N/A	71.4
Capture	0.4078	2545.3	0.4315	2050.2	0.4327	1936.9	0.4337	1785.1	0.4352	1593.3
(n,2n)	0.0008	4.3	0.0007	3.5	0.0007	3.5	0.0007	3.5	0.0007	3.5
Total sum (pcm)	1437.1		1348.5		1252.8		1117.3		938.7	

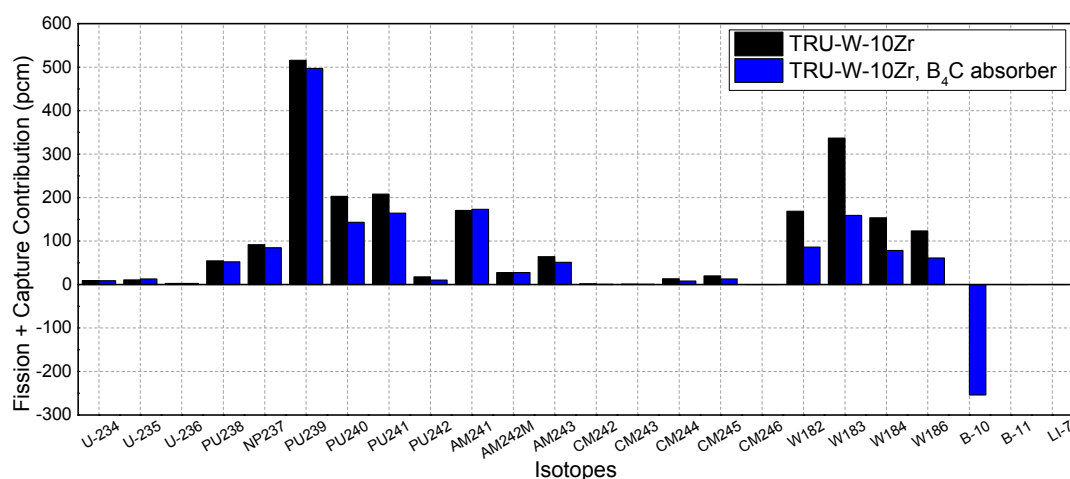


**Figure 7.** Comparison of nuclide-wise contribution to sodium void reactivity worth (BOEC).

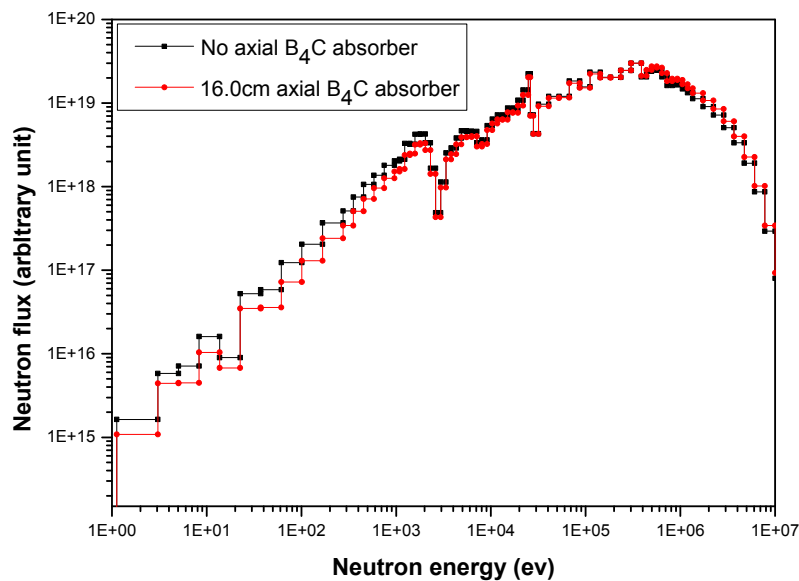


Figure 8. Comparison of the neutron spectra for two uranium-free cores (BOEC).

### 3.3. Quasi-Static Reactivity Balance Analysis

We performed the quasi-static reactivity balance analysis to understand and check the safety features of the advanced uranium-free fueled cores proposed in this work. This quasi-static reactivity balance analysis methodology [4,16,23] was first developed by Wade and Hill to check if the SFR core has passive self-controllability under ATWS (anticipated transients without scram) like unprotected loss-of-flow transient (ULOF), unprotected loss-of-heat-sink (ULOHS), and unprotected transient overpower (UTOP). This self-controllability means that a reactor leads to a passive safe shutdown state only through the reactivity feedback effects (i.e., Doppler effect, fuel axial expansion, radial expansion of core support plate, coolant thermal expansion effect, and so on) without exceeding the limits, ensuring that core integrity can be used as a measure of the inherent safety features of the cores. To meet this, the six self-controllability parameters for sodium-cooled fast reactor should be satisfied (See Table 8). The parameters given in Table 8 are associated with the reactivity coefficients as follows:

$$\begin{aligned}
 A &= (\alpha_D + \alpha_e)\Delta T_f, \\
 B &= (\alpha_D + \alpha_e + \alpha_{co} + 2\alpha_{RD} + 2\alpha_R)\Delta T_C/2, \\
 C &= \alpha_D + \alpha_e + \alpha_{co} + \alpha_R.
 \end{aligned}
 \tag{4}$$

In Equation (4),  $\alpha_D$ ,  $\alpha_e$ ,  $\alpha_{co}$ ,  $\alpha_{RD}$ , and  $\alpha_R$  represent the Doppler coefficient, the fuel axial expansion reactivity coefficient, the coolant expansion reactivity coefficient, the control rod driveline thermal expansion reactivity coefficient, and the core radial expansion reactivity coefficient, respectively.  $\Delta T_f$  and  $\Delta T_c$  are the incremental temperature increase in the fuel and the full power steady-state coolant temperature increase, respectively. In this work,  $\Delta T_f$  and  $\Delta T_c$  were assumed to be 150 °C and 155 °C, respectively.  $\rho_{TOP}$  is the maximum reactivity insertion due to a control rod runout and we additionally considered 20% uncertainty for burnup reactivity swing.

**Table 8.** Results of quasi-static reactivity balance analysis for cores having different axial B<sub>4</sub>C absorber region heights.

Height of B <sub>4</sub> C Absorber Region	No Absorber Region	10.0 cm	11.4 cm	13.3 cm	16.0 cm
A (pcm, <0)	−114/−126 <sup>a</sup>	−83/−90	−78/−84	−74/−79	−70/−75
B (pcm, <0)	−132/−144	−133/−142	−138/−146	−147/−156	−158/−168
C (pcm/°C, <0)	−1.019/−1.118	−0.950/−1.012	−0.977/−1.040	−1.040/−1.109	−1.127/−1.207
A/B (≤1)	0.864/0.875	0.624/0.636	0.562/0.572	0.504/0.511	0.442/0.446
(1≤) CΔT <sub>c</sub> /B (≤2)	1.197/1.202	1.103/1.108	1.096/1.101	1.099/1.105	1.104/1.112
ρ <sub>TOP</sub> / B  (≤1)	1.646/NA	1.172/NA	1.120/NA	1.044/NA	0.964/NA

<sup>a</sup> BOEC/EOEC.

As shown in Table 8, all the cores satisfy all the criteria for self-controllability except for the last criterion associated with UTOP both at BOEC and EOEC, while the last core having 16.0 cm thick B<sub>4</sub>C absorber regions satisfies all the criteria of self-controllability due to the improvement of the core performance.

Finally, we close this section by evaluating the shutdown margin of the primary control rod assemblies to show that this core has a sufficient shutdown margin even if the B<sub>4</sub>C absorber region reduces the reactivity worth of the control rod assemblies. Table 9 summarizes the detailed results of shutdown margin evaluation for the core having a 16.0 cm thick B<sub>4</sub>C absorber. The temperature defect, which means the reactivity change from the hot full power to refueling states, was estimated to be 459 pcm and the one stuck assembly worth was estimated to be relatively high (i.e., 1043 pcm). The largest portion of the required reactivity component is the fuel cycle excess reactivity, which is the burnup reactivity swing including 20% uncertainty. It was shown that primary control assemblies have a sufficient shutdown margin of 3863 pcm.

**Table 9.** Shutdown margin of the core having axial B<sub>4</sub>C absorber regions (BOEC, 16.0 cm thick B<sub>4</sub>C absorber).

Height of B <sub>4</sub> C Absorber Region	16.0 cm
Temperature defect (pcm)	459
Full power to hot standby (pcm)	153
Hot standby to refueling (pcm)	306
Overpower (15%) (pcm)	23
Fuel cycle excess reactivity (pcm)	4088
Uncertainty (pcm)	926
Temperature defect (20%) (pcm)	92
Burnup reactivity (20%) (pcm)	818
Criticality Prediction (pcm)	300
Fissile loading (pcm)	300
Reactivity fault (pcm)	438
Total reactivity worth (pcm)	10839
One stuck assembly worth (pcm)	1043
Reactivity worth available (pcm)	9796
Maximum reactivity requirement (pcm)	5933
Shutdown margin (pcm)	3863

#### 4. Fuel Cycle Analysis

In this section, the performance of the fuel cycle, which is comprised of a PWR and SFR burner, is analyzed and compared with that of the once-through PWR fuel cycle. In the once-through PWR fuel cycle option, a batch of depleted fuel is discharged at the end of each cycle and then the discharged fuels go to the repository after cooling. In this work, we assumed the average burnup of the discharged fuels for PWR is 50 MWD/kg and the initial uranium enrichment of them is 4.5 wt %. The second fuel cycle represents the combination of the PWR and SFR burner. In this fuel cycle, the discharged

PWR spent fuel after 10 years' cooling is reprocessed using pyro-processing and then fed into the SFR core after mixed with the recycled SFR actinide fuel. The discharged fuels from SFR burner core are sent to the reprocessing plant where the recovery factors for actinides and rare earth fission products are assumed to be 99.9% and 5%, respectively, while all the other fission products are assumed to be completely removed. Then, the recovered fuels from reprocessing are sent to the fuel fabrication plant, where they are mixed with TRU nuclides fed from PWR spent fuel. For the second fuel cycle analysis, the SFR core (Case V in Table 6) having TRU-W-10Zr fuel and 16.0 cm thick B<sub>4</sub>C absorber region was considered as the SFR burner core. The basic fuel cycle data used in this work are summarized in Table 10.

**Table 10.** Main parameters of the fuel cycles.

Fuel Cycle	Once-Trough	PWR-SFR
Electric power (MWe)	1000	400
Thermal efficiency (%)	34.23	39.4
U-235 Enrichment (wt %)	NU: 0.71% <sup>a</sup> DU: 0.25% <sup>b</sup> EU: 4.5% <sup>c</sup>	NU: 0.71% DU: 0.25% EU: 4.5%
PWR Fuel burnup (MWD/kg)	50.0	50.0
SFR fuel type		TRU-W-10Zr
SFR Burnup (MWd/kg)	-	161
Electric Energy (TWhe)		
PWR	1.0	0.788
SFR	-	0.212
Recovering factors (Pyro-Processing)		
U	-	100%
TRU	-	99.9%
RE	-	5%
Recovery factor during fuel fabrication	99.9%	99.9%
Recovery factor during Conversion	99.9%	99.9%

<sup>a</sup> Natural uranium, <sup>b</sup> Depleted uranium, <sup>c</sup> Enriched uranium.

For the two considered fuel cycles, the total electricity produced from all the reactors is normalized to 1 TWhe. First, with the equilibrium conditions, we analyzed the mass flows through all the components contained in the fuel cycles [2,24]. The results of mass flow analyses are shown in Figure 9. For the once-through PWR cycle, 22.49 tons of natural uranium are required and 2.435 tons of enriched uranium are fed into PWR, while 2.309 tons of spent fuel are discharged. For the PWR–SFR fuel cycle option, the natural uranium requirement is reduced to ~17.725 tons and the amount of enriched uranium is also reduced to ~1.919 tons due to the reduction of electricity generation by PWR. The charged TRU mass for SFR is composed of 0.02398 tons from PWR spent fuel and 0.1122 tons from recycled fuel of SFR burner spent fuel, while the charged uranium for SFR is composed of 0.0031 tons from recycled fuel of SFR burner spent fuel. The total amount of TRU wastes going to repository for this fuel cycle option is ~0.000136 tons, which is drastically smaller than that of the once-through PWR option (i.e., 0.0305 tons). For uranium, the PWR–SFR fuel cycle option has a smaller amount of uranium waste of 1.7959 tons (from the reprocessed PWR spent fuel) than that of the once-through PWR option (i.e., 2.2787 tons). However, it is noted that the amounts of fission product (FP) wastes are similar to each other because FP generation is nearly proportional to the thermal energy generated by fission. Also, this mass flow analysis showed that the SFR burner produces only 0.2119 TWhe, which is just about 1/3.72 of the electricity produced by PWR. This means that one SFR burner can consume TRUs discharged from 3.72 PWRs, producing the same electricity. The factor is different from the support ratios that are given in Section 3 because the support ratios in Section 3 were evaluated based on the thermal output.

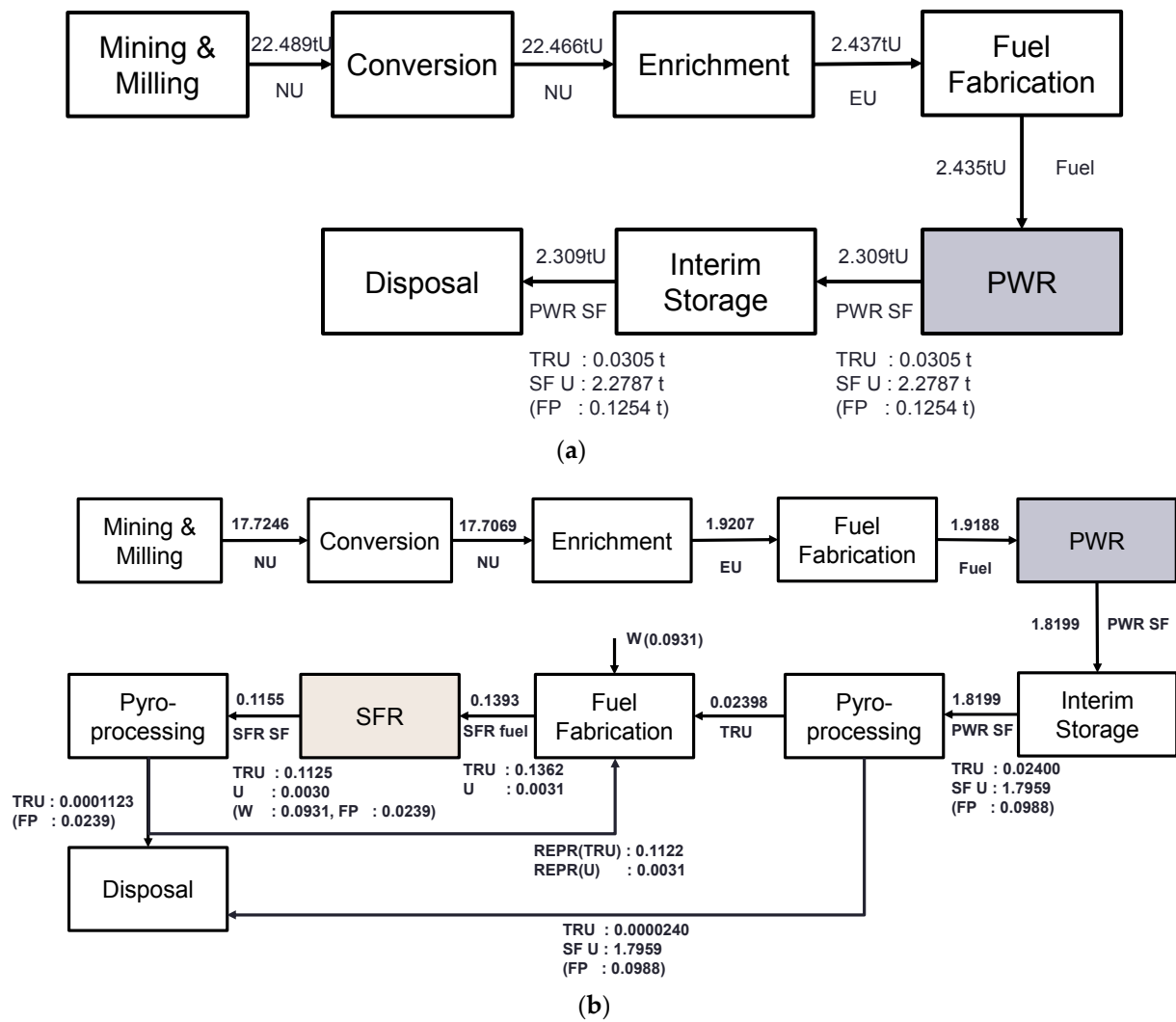


**Figure 9.** Comparison of the mass flows for two fuel cycle options (mass unit: tons). (a) PWR Once-Through (OT) cycle (PWR: 1TWhe); (b) PWR-SFR cycle (PWR: 0.788 TWhe, SFR: 0.212 TWhe).

Figure 10 compares the evolutions of the radioactivity of the wastes going to repository for two fuel cycle options described above, while Figure 11 shows the evolution of the decay heat of the wastes for three different fuel cycle options. As shown in Figures 10 and 11, in comparison with the once-through PWR option, the PWR-SFR coupling cycle option drastically reduces the radioactivity and the decay heat of the waste. In particular, the radioactivity of the wastes going to the repository for the PWR-SFR coupling option is reduced by a factor of  $\sim 10^7$  of the initial value within the time period less than 1000 years while the one for the once-through PWR option is still higher by approximately two orders of magnitude even at 1000 years after discharge than those of the PWR-SFR coupling option. Figure 11 shows that the decay heat of the wastes for the PWR-SFR is lower by two orders of magnitude than the PWR once-through option at 1000 years after discharge. The decomposition of radioactivity of the wastes in Figure 10b for the PWR-SFR coupling option shows that the main contributions are from the FPs of the PWR spent fuel and the radioactivities of TRU wastes are much lower than those of the FP wastes and they monotonically decrease as time passes. On the other hand, the decomposition of the waste decay heat for the PWR-SFR coupling option in Figure 11b shows that the decay heats from FP waste are initially much higher than those of TRU wastes but they make only a minor contribution to the total decay heat after 1000 years. These reductions in the radioactivity and decay heat for the wastes of PWR-SFR option are similar to the results given in other studies [1–3,21].

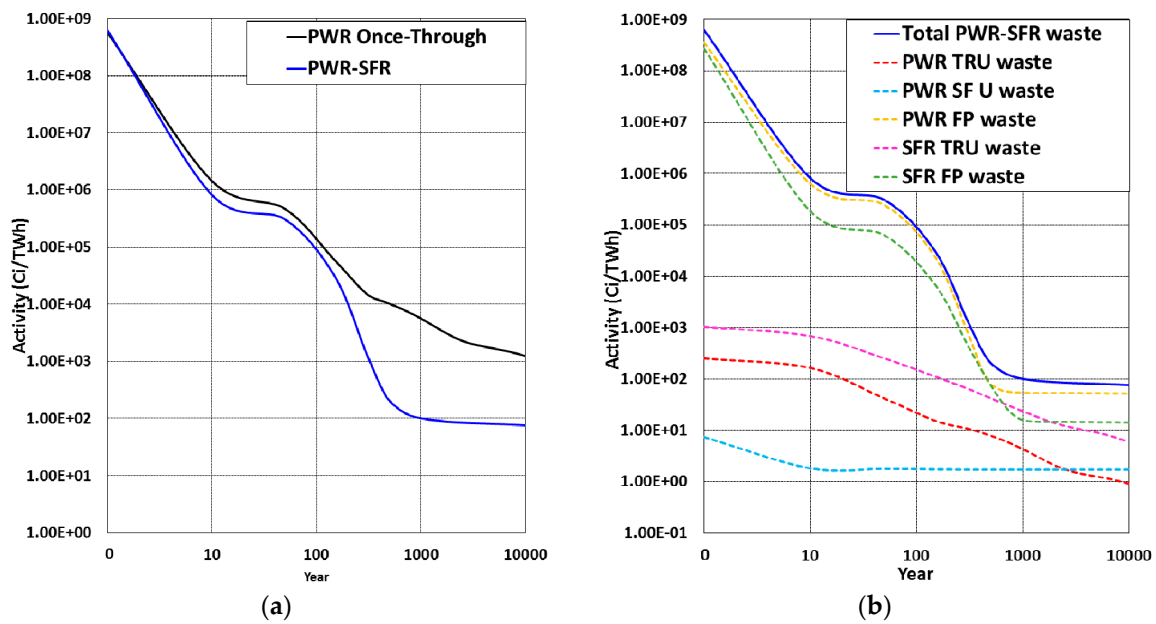


**Figure 10.** Comparison of the evolutions of radioactivity of wastes for different fuel cycles: (a) PWR versus PWR-SFR; (b) decomposition of radioactivity for PWR-SFR.

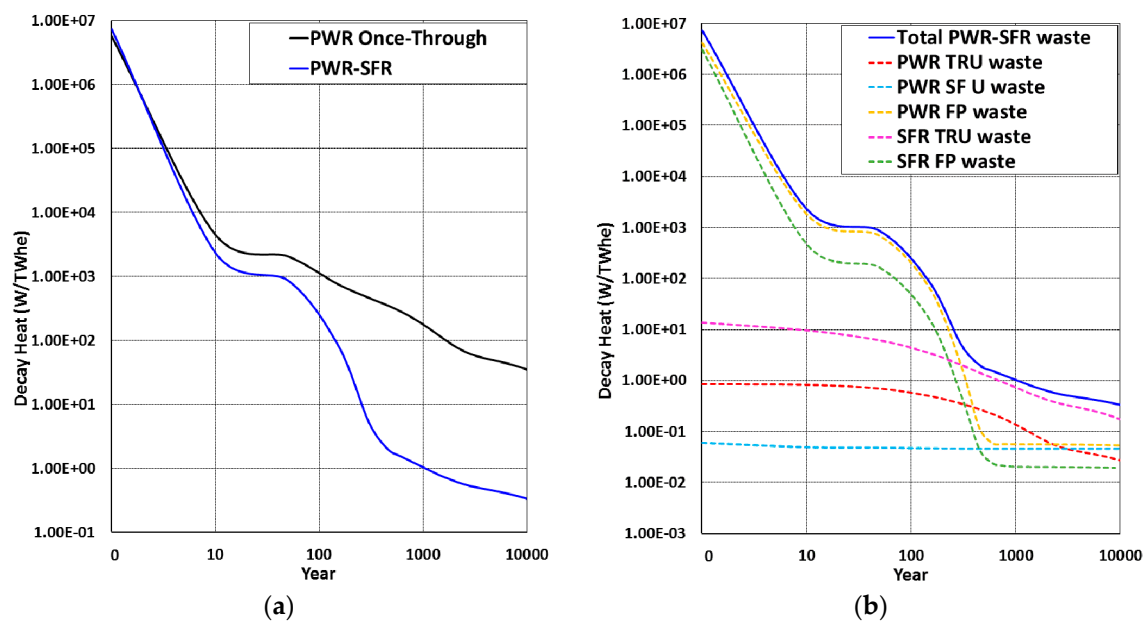


**Figure 11.** Comparison of the evolutions of decay heat of wastes for different fuel cycles: (a) PWR versus PWR-SFR; (b) decomposition of decay heat for PWR-SFR.

## 5. Summary and Conclusions

In this work, uranium-free fueled SFR burner cores were suggested to maximize the TRU burning rate with improvement of safety-related parameters such as the reactivity coefficients including Doppler coefficient and burnup reactivity swing by using resonance nuclides such as nickel and tungsten and with an axially central  $B_4C$  absorber region. The analysis of the reference cores using different metallic fuels showed that, in spite of its high TRU burning rate, the reference burner core using the binary metallic fertile-free fuel (i.e., TRU-Zr) has a very small Doppler coefficient and large burnup reactivity swing, which can be problematic in terms of safety, while this core has the smallest

sodium void worth, even smaller than that of the ternary metallic fertile fueled core (i.e., TRU-U-10Zr). In this work, the previous decomposition method based on the neutron balance and normalization to the fission production rate was extended to further decompose the fission term into fission production and the capture contributions via fission. The decomposition analysis of sodium void worth showed that the smallest sodium void worth of the reference core using TRU-U-10Zr resulted from the largest negative contribution of the neutron leakage increase, in spite of the largest positive contribution of capture decrease under sodium voiding. On the other hand, the reference cores using two resonant nuclides (i.e., tungsten and nickel) have improved more negative Doppler coefficients and significantly reduced burnup reactivity swing compared to the reference core using TRU-Zr fuel. In particular, the reference core using TRU-W-10Zr fuel showed the most negative Doppler coefficient and smallest burnup reactivity swing, while it has the largest sodium void worth due to the large capture resonance cross sections of tungsten isotopes. This smallest burnup reactivity swing resulted from the large initial heavy metal inventory and the largest sodium void worth is due to the smallest negative contribution by leakage increase under sodium voiding. In this work, an axial B<sub>4</sub>C region was considered to be placed in the axially central region of the core using TRU-W-10Zr in order to further improve the burnup reactivity swing and reduce sodium void reactivity and 12 ZrH<sub>2</sub> moderator rods are added for each fuel assembly to further improve the Doppler effect and the sodium void worth. The results of the analysis showed that the core having a 16 cm high B<sub>4</sub>C absorber region has reduced values of burnup reactivity swing and sodium void worth (by 1736 pcm and 498 pcm, respectively) in comparison with the core having no B<sub>4</sub>C absorber region. On the other hand, it was shown that this core has less negative Doppler coefficients due to its reduced amount of resonant nuclide (i.e., W) and the reduced worth of the primary control rods. The quasi-static reactivity balance analysis for the burner cores having different height of the B<sub>4</sub>C absorber region showed that the core having 16.0 cm thick B<sub>4</sub>C absorber region satisfies all the criteria for the self-controllability under the unprotected accidents and its primary control assemblies have sufficient shutdown margin. The comparative fuel cycle analysis performed for the once-through PWR and the PWR-SFR burner coupling options showed that the PWR-SFR burner coupling option significantly reduces the amount of TRU waste going to repository by a factor of ~224. The radioactivity and decay heat of the wastes going to the repository for this PWR-SFR burner coupling option are reduced to 1/10<sup>7</sup> of their initial values, while those of the PWR once-through option are higher by two orders of magnitude than the PWR-SFR option within 1000 years after discharge. In particular, it is shown from the mass flow analysis for the PWR-SFR burner coupling option that the fertile-free SFR burner core can consume the amount of TRUs that is discharged from ~3.72 PWRs of the same electricity output.

From these results, it can be concluded that the fertile-free fueled SFR burner core suggested in this work is not only neutronicly feasible and promising in terms of reducing TRU waste of the PWR spent fuel stock but also has inherent safety features in terms of self-controllability.

**Acknowledgments:** This work was supported by the National Research Foundation (NRF) of Korea through project No. NRF-2017M2A8A6017972 and was also partially supported by “Human Resources Program in Energy Technology” of the Korea Institute of Energy Technology Evaluation and Planning (KETEP) granted financial resource from the Ministry of Trade, Industry & Energy, Republic of Korea (No. 20164030200990).

**Author Contributions:** Wuseung You designed and analyzed the advanced sodium-cooled fast reactor cores using uranium-free metallic fuels including the fuel cycle analysis with the guidance of Prof. Ser Gi Hong. Ser Gi Hong as the advisor suggested ideas and directions for this work.

**Conflicts of Interest:** The authors declare no conflict of interest.

## References

1. Salvatores, M.; Palmiotti, G. Radioactive waste partitioning and transmutation within advanced fuel cycles: Achievements and challenges. *Prog. Part. Nucl. Phys.* **2011**, *66*, 144–166. [[CrossRef](#)]
2. Nuclear Energy Agency. *Accelerator-Driven Systems (ADS) and Fast Reactors (FR) in Advanced Fuel Cycle*; NEA-3109; Nuclear Energy Agency: Paris, France, 2002.

3. Salvatores, M. Transmutation: Issues, innovative options and perspective. *Prog. Nucl. Energy* **2002**, *40*, 375–402. [[CrossRef](#)]
4. Wade, D.C.; Chang, Y.I. The integral fast reactor concept: Physics of operation and safety. *Nucl. Sci. Eng.* **1987**, *100*, 507–524. [[CrossRef](#)]
5. Yang, W.S. Fast Reactor Physics and Computational Methods. *Nucl. Eng. Technol.* **2012**, *44*, 177–198. [[CrossRef](#)]
6. Tommasi, J.; Delpech, M.; Grouiller, P.; Zaetta, A. Long-lived waste transmutation in Reactors. *Nucl. Technol.* **1995**, *111*, 133–148. [[CrossRef](#)]
7. Languille, A.; Gamier, J.C.; Lo Pinto, P.; Na, B.C.; Verrier, D.; Deplaix, J.; Allan, P.; Newton, T.; Sunderland, R.E.; Kiefhaber, E. CAPRA Core studies—The oxide reference option. In Proceedings of the International Conference on Evaluation of Emerging Nuclear Fuel Cycle Systems, Paris, France, 11–14 September 1995.
8. Rouault, J.; Garnier, J.C.; Languille, A.; Lo Pinto, P. The design of U-free large fast reactor cores. The CAPRA program trends. In Proceedings of the International Conference on the Physics of Reactors (PHYSOR96), Mitto, Japan, 16–20 September 1996.
9. Filin, A.I.; Orlov, V.V.; Leonov, V.N.; Sila-Novitskij, A.G.; Smirnov, V.S.; Tsikunov, V.S. Design features of BREST reactors. Experimental work to advance the concept of BREST reactors. Results and plans. In Proceedings of the International Conference on Future Nuclear Systems, Jackson Hole, WY, USA, 29 August–3 September 1999.
10. Merk, B.; Stanculescu, A.; Chellapandi, P.; Hill, R. Progress in reliability of fast reactor operation and new trends to increased inherent safety. *Appl. Phys.* **2015**, *147*, 104–116. [[CrossRef](#)]
11. Coz, P.L.; Sauvage, J.F.; Serpantie, J.P. Sodium-cooled fast reactors: The ASTRID plant project. In Proceedings of the International Congress on Advances in Nuclear Power Plants (ICAPP2011), Nice, France, 2–6 May 2011.
12. Lee, C.B.; Cheon, J.S.; Kim, S.H.; Park, J.Y.; Joo, H.K. Metal fuel development and verification for prototype generation IV sodium-cooled fast reactor. *Nucl. Eng. Technol.* **2016**, *48*, 1096–1108. [[CrossRef](#)]
13. Hong, S.G.; Kim, S.J.; Kim, Y.I. Annular fast reactor cores with low sodium void worth for TRU burning. *Nucl. Technol.* **2008**, *162*, 1–25. [[CrossRef](#)]
14. You, W.; Hong, S.G. A core physics study of advanced sodium-cooled TRU burners with thorium—And uranium-based metallic fuels. *Nucl. Technol.* **2016**, *194*, 217–232. [[CrossRef](#)]
15. You, W.; Hong, S.G. A neutronic study on advanced sodium cooled fast reactor cores with thorium blankets for effective burning of transuranic nuclides. *Nucl. Eng. Des.* **2014**, *278*, 274–286. [[CrossRef](#)]
16. Romano, A.; Hejzlar, P.; Todreas, N.E. Fertile-free fast lead-cooled incinerators for efficient actinide burning. *Nucl. Technol.* **2004**, *147*, 368–387. [[CrossRef](#)]
17. Nessaoudi, N.; Tommasi, J. Fast burner reactor devoted to minor actinide incineration. *Nucl. Technol.* **2002**, *137*, 84–96. [[CrossRef](#)]
18. Wakabayashi, T.; Takahashi, K.; Yanagisawa, T. Feasibility studies on plutonium and minor actinide burning in fast reactors. *Nucl. Technol.* **1997**, *118*, 14–25. [[CrossRef](#)]
19. Krivitski, I.; Vorotyntsev, M.; Pyshin, V.; Korobeinikova, L. Safety analysis of fast reactor core with uranium-free fuel for actinide transmutation. *Nucl. Technol.* **2003**, *143*, 281–289. [[CrossRef](#)]
20. You, W.; Hong, S.G. Sodium-cooled fast reactor cores using uranium-free metallic fuels for maximizing TRU support ratio. In Proceedings of the Korean Nuclear Society Autumn Meeting, Pyeongchang, Korea, 30–31 October 2014.
21. Sun, K.; Krepel, J.; Mikityuk, K.; Pelloni, S.; Chawla, R. Void reactivity decomposition for the sodium-cooled fast reactor in equilibrium fuel cycle. *Ann. Nucl. Energy* **2011**, *38*, 1645–1657. [[CrossRef](#)]
22. Kim, D.Y.; Hong, S.G.; Park, C.J. Coupling of an innovative small PWR and advanced sodium-cooled fast reactor for incineration of TRU from once-through PWRs. *Int. J. Energy Res.* **2016**, *40*, 216–229. [[CrossRef](#)]
23. Wade, D.C.; Hill, R.N. The design rationale for the IFR. *Prog. Nucl. Energy* **1997**, *31*, 13–42. [[CrossRef](#)]
24. Fao, F.; Ko, W.L. Modeling and system analysis of fuel cycles for nuclear power sustainability (I): Uranium consumption and waste generation. *Ann. Nucl. Energy* **2014**, *62*, 10–23.
25. MacFarlane, R.E. *TRANSX 2: A Code for Interfacing MATXS Cross Section Libraries to Nuclear Transport Codes*; LA-12312-MS; Los Alamos National Laboratory: Los Alamos, NM, USA, 1993.

26. Derstine, K.L. *DIF3D10.0: Code System Using Variational Nodal Methods and Finite Difference Methods to Solve Neutron Diffusion and Transport Theory Problems*; CCC-784; Argonne National Laboratory: Argonne, IL, USA, 2011.
27. Toppel, B.J. *A User's Guide for the REBUS-3 Fuel Cycle Analysis Capability*; ANL-83-2; Argonne National Laboratory: Lemont, IL, USA, 1992.
28. Merk, B. Moderating material to compensate the drawback of high minor actinide containing transmutation fuel on the feedback effects in SFR cores. *Sci. Technol. Nucl. Install.* **2013**, *3*, 21–30. [[CrossRef](#)]



© 2017 by the authors. Licensee MDPI, Basel, Switzerland. This article is an open access article distributed under the terms and conditions of the Creative Commons Attribution (CC BY) license (<http://creativecommons.org/licenses/by/4.0/>).